Data in Brief 20 (2018) 2054–2064

Contents lists available at ScienceDirect

Data in Brief

journal homepage: www.elsevier.com/locate/dib

Data Article

Experimental and theoretical structural/spectroscopical correlation of enterobactin and catecholamide

M. Moreno [b,*], A. Zacarias [a,*], L. Velasquez [c,h], G. Gonzalez [d,e], M. Alegría-Arcos [f,g], F. Gonzalez-Nilo [f], E.K.U. Gross [a]

[a] Max Planck Institute of Microstructure Physics, Weinberg 2, D06120 Halle, Germany and ETSF.
[b] University of the Basque Country, Barrio Sarriena, s/n, 48940 Leioa, Bizkaia, Spain
[c] Universidad Andres Bello, Facultad de Medicina, Center for Integrative Medicine and Innovative Science, Echaurren 183, Santiago, Chile
[d] Center for Development of Nanoscience and Nanotechnology, CEDENNA, Casilla 653, Santiago, Chile
[e] Universidad de Chile, Facultad de Ciencias, Departamento de Química, Laboratorio de Sintesis Inorganica y electroquímica, Las Palmeras 3425, Nuñoa, Santiago, Chile
[f] Universidad Andres Bello, Facultad de Ciencias Biologicas, Center for Bioinformatic and Integrative Biology, Av Republica 239, Santiago, Chile
[g] Centro Interdisciplinario de Neurociencias de Valparaíso (CINV), Facultad de Ciencias, Universidad de Valparaíso, Valparaíso, Chile
[h] Facultad Ciencias de la Salud, Universidad SEK, Chile, Fernando Manterola 0789, Providencia, Santiago

ARTICLE INFO

Article history:
Received 23 February 2018
Received in revised form
9 May 2018
Accepted 24 August 2018
Available online 29 August 2018

Keywords:
Catecholate FeEnterobactin
FTIR
DFT
MD

ABSTRACT

Here we report the IR spectra of FeEnterobactin in catecholate conformations ($[CatFeEB]^{3-}$) obtained by DFT calculations using PBE/QZVP and their correlation it with its experimental counterpart $[SalH_3FeEB]^0$. Fragments of FeEnterobactin and Enterobactin (H_6EB) are elucidated from their MALDI-TOF mass spectrometry, and the dependence of the frontier orbitals (HOMO and LUMO) with the catecholamide dihedral angles of H_6EB is reported. The frequency distribution of catecholamide dihedral angle of H_6EB was carried-out using molecular dynamics (MD). The data presented enriches the understanding of $[CatFeEB]^{3-}$ and H_6EB frequency distribution and reactivity.

DOI of original article: https:doi.org/10.1016/j.saa.2018.02.060
* Corresponding authors.
E-mail addresses: mmoreno043@ikasle.ehu.eus (M. Moreno), zacarias@mpi-halle.mpg (A. Zacarias).

https:doi.org/10.1016/j.dib.2018.08.114

Specifications table

Subject area	Chemistry and biology.
More specific subject area	Synthesis, Functionalization, and Characterization of FeEnterobactin and Enterobactin, IR spectra, catecholamide dihedral angles distribution and reactivity.
Type of data	Plots were done with Origin 6.0 (OriginLab, Northampton, MA). We used Gauss-View to visualize the frontier orbitals, density, electrostatic potentials and vibrational modes.
How data was acquired	DFT calculations using PBE exchange/correlation functionals and QZVP basis set were used to obtain the infrared spectra (IR) of $[SalFeH_3EB]^0$ and H_6EB. Experimental IR were recorded on a Brucker IFS66v/S vacuum FTIR spectrometer with a Ge/KBr beam splitter and DTGS detector, and the MALDI-TOF MS spectra were acquired with an Ultraflex II TOF-TOF mass spectrometer (Bruker Daltonics) for both samples (more details in *Spectrochim. Acta A (2018) 198, 264–277*). To obtain the frequencies distribution of different dihedral angles values (Arm1, Arm2, and Arm3, see Figs. 1-7) from H_6EB structures over a time lapse, we used the Desmond code [4] to perform the molecular dynamics (MD) simulations for the four structures of H_6EB. Each structure was embedded into an explicit TIP3P 2water box. The NPT ensemble was employed with at 300 K and 1.01 bar of pressure and the OPLS-2005 Force Field 3were used 4. Before the MD simulations, the energy of each system was minimized and then, MD simulations were carried out for 5 ns. We used a VMD program [5] to calculate the dihedrals angles on the catecholamides for the H_6EB structures during the MD trajectory. Plots were done with Origin 6.0 (OriginLab, Northampton, MA). All systems were simulated considering periodic boundary conditions (PBC).
Data format	Figs. in TIF format.
Experimental factors	Experimental IR were recorded at 50000 scans with 2 cm^{-1} resolution. The sample, $[SalFeH_3EB]^0$ were prepared using KRS-5 disc. fifty milligrams of $[SalFeH_3EB]^0$ and H_6EB, separately, was dispersed in 100 μl of dichloromethane, then one drop was placed on a KRS-5 disc to dry. Solid $[SalFeH_3EB]^0$ was characterized. All solvents were of analytical purity. For the sample preparation of MALDI-TOF MS spectra, 0.5 mL of a saturated solution of a-cyano-4-hydroxycinnamic acid (HCCA) in acetone was deposited on the sample target. A 1 ml aliquot of the sample was injected into a small drop of water previously deposited on the matrix surface [1].
Experimental features	Infrared Spectra of $[SalFeH_3EB]^0$ was carried out on solid state at RT, instead, a liquid state is performed to capture MALDI-TOF MS spectra.
Data source location	Theory and Experimental II departments of the Max Planck Institute of Microstructure Physics, Halle/Germany. Universidad Andres Bello, Facultad de Ciencias Biologicas, Center for Bioinformatic and Integrative Biology (CBIB).
Data accessibility	Data described here are Supplementary information to the article entitled “IR and NMR Spectroscopic Correlation of Enterobactin by DFT” Spectrochimica Acta A (2018) [1].

Related research article	Major details about Enterobactin IR spectra can be found in "IR and NMR Spectroscopic Correlation of Enterobactin by DFT" Spectrochimica Acta A (2018) [1] The Functionalization and characterization of Enterobactin and Fe Enterobactin analogs as well as their affinity prediction with FepA-protein transmembrane using DFT, Molecular Dynamics and Docking will be reported elsewhere.

Value of the data

- The elucidation of ($[CatFeEB]^{3-}$) IR spectra by DFT contrasted with experimental IR leads a greater understanding of the functional group motion which favors the explanation of their chemical modification.
- The determination of the frequency distribution of dihedral angles of H_6EB structures using molecular dynamics (MD) allows to reveal the predominant structure and with this, its prevailing electronic properties; their reactivity parameters leads to predict synthesis of new materials.
- The visualization of atomic bond cleavage of FeEnterobactin and Enterobactin obtained by mass spectrometry permit determine the reactivity sites useful for the implementation of functionalization methodologies.

1. Data

Fig. 1 shows the calculated catecholate FeEnterobactin ($[CatFeEB]^{3-}$) contrasted with experimental $[SalFeH_3EB]^0$.

Unlike the H_6EB [1], the calculated $[CatFeEB]^{3-}$ shows a unique broad and sharp N-H band at 3547 cm^{-1}, coherent with steric restrictions associated to the Fe, and as it is expected the stretching OH bands localized at 3812, 3846, 3747, 3522, 3420, 3371, 3221 and 2880 cm^{-1} in H_6EB

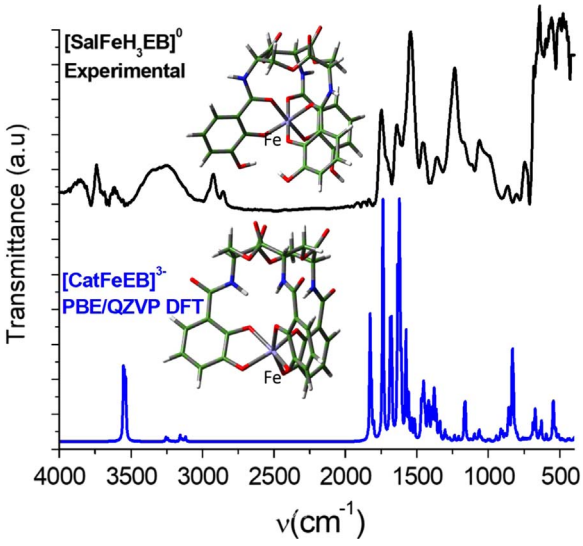

Fig. 1. Calculated $[CatFeEB]^{3-}$ IR spectra using PBE/QZVP method and Experimental $[SalFeH_3EB]^0$ in the range of 4000–450 cm^{-1}. $[CatFeEB]^{3-}$ corresponds to Fe linked at catechol groups, and $[SalFeH_3EB]^0$ to Fe at catecholamide groups respectively.

disappear in calculated $[CatFeEB]^3$. Instead, this band is present in experimental FeEnterobactin, associated to the Fe linked in the Salicylate conformation $[SalFeH_3EB]^0$ as it is reported by N.K. Raymond [10,11]. In the case of stretching and bending C-O bands its intensity decreases, and/or in some cases a signal shift is observed for 1336, 1235, 1175, 1125, 1032, 980, 849, 801, 695, 535 to

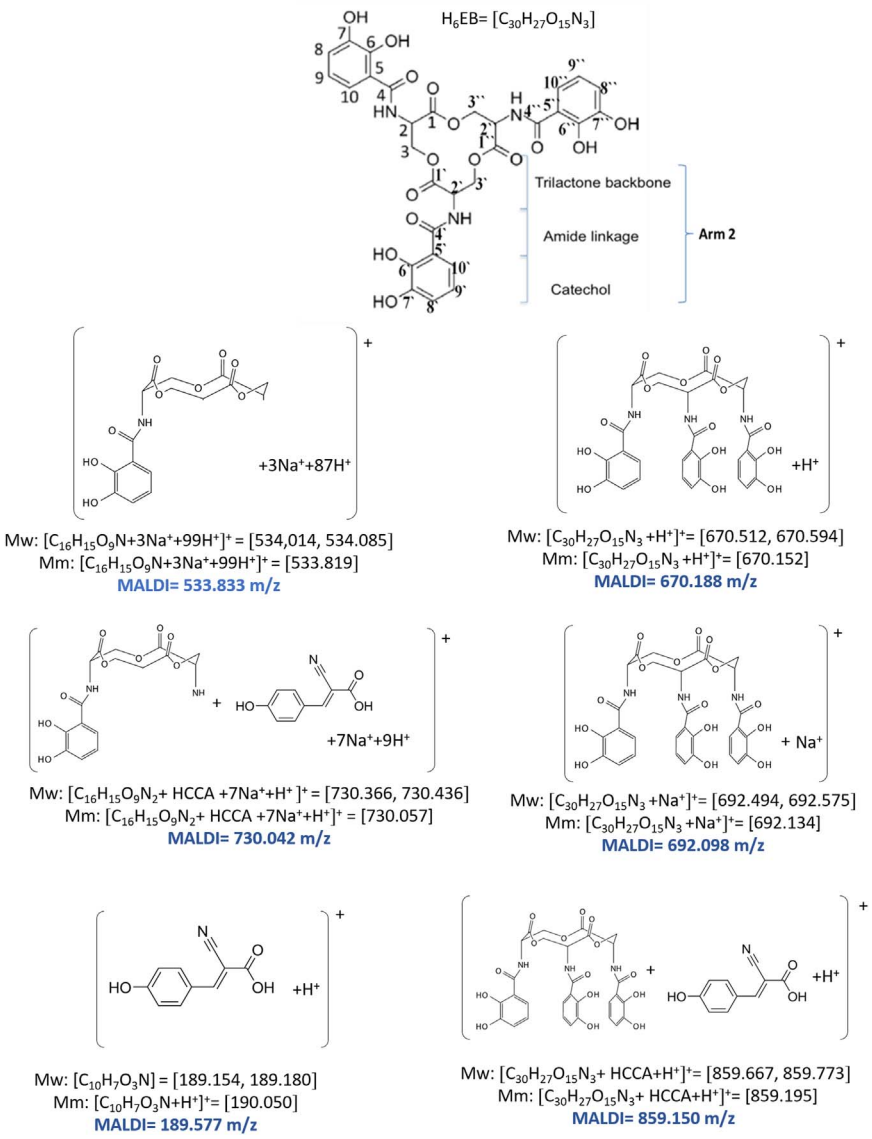

Fig. 2. H_6EB fragments based on MALDI-TOF MS spectra [1], calculated using minimum and maximum atomic weights (ma) from the IUPAC 2013 technical report [12], and Mm (monoisotopic mass) [16]. $m_a(H)$= [1.00784, 1.00811]; $m_a(C)$[12.0096, 12.0116], $m_a(N)$ [14.00643, 14.00728], $m_a(O)$[15.99903, 15.99977] and $m_a(Na)$[22.98977] were considered in the estimation of minimum and maximum molecular weights (Mw), and Mm was calculated using web tool provides by http://www.cheminfo.org. Being the average of the mass measurement error (or accuracy) of Δm:33.031 ppm (0.0033%) [16].

1378, 1361, 1094, 1064, 990, 943, 913, 857, 673, 629 and 544 cm^{-1} in $[CatFeEB]^{3-}$, details of the H_6EB IR can be found in [1]. $[CatFeEB]^{3-}$ data revels signal shifts for the stretching (C=C) IR bands from 1587, 1544, 1468, 1390, 1343 to 1574, 1555, 1466, 1450, 1370 and 1335 cm^{-1}, respectively, this is due to the inductive effect of the Fe attached to the catechol groups, similar to the reports from N.K. Raymond [10,11]. The IR data is used as guide to improve the elucidation of FeEnterobactin and analogs. MALDI-TOF MS data of $[CatFeEB]^{3-}$ exhibits a cleavage in C5-C4 instead C4-N in H_6EB, again, it seems to be that the steric restrictions of the Fe linked to catechol

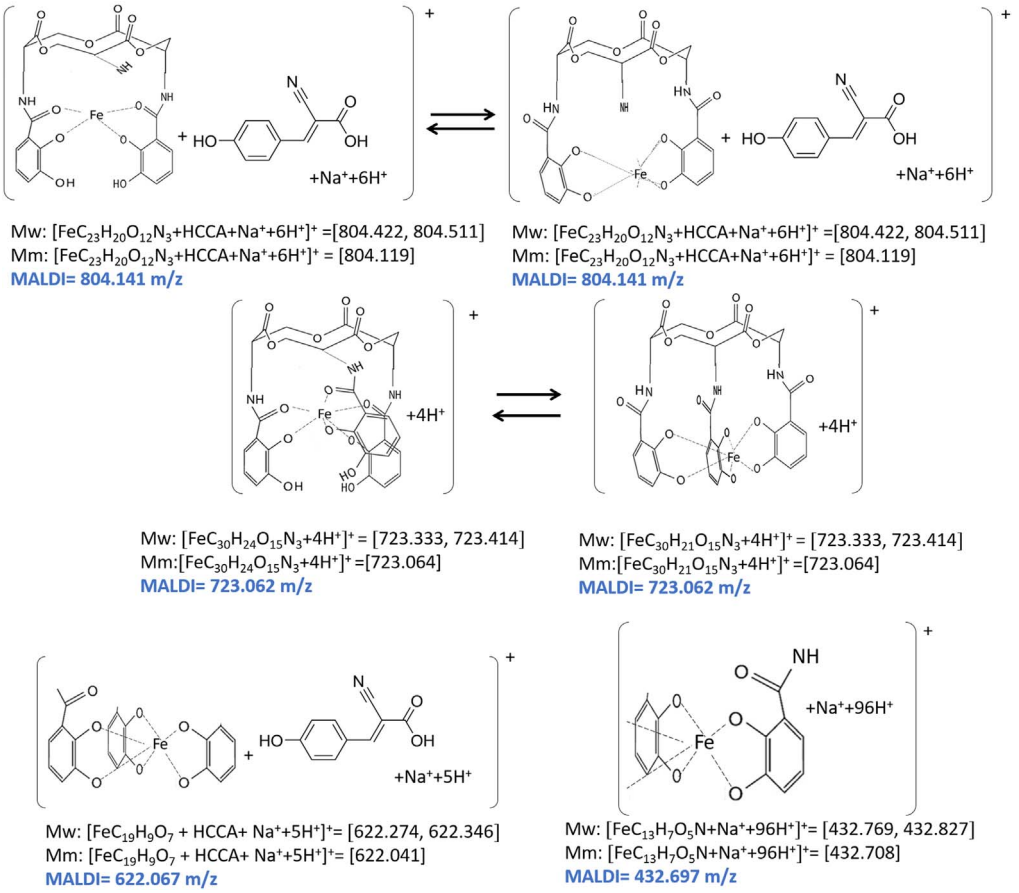

Fig. 3. CatFeEnterobactin (CatFeEB) and SalFeH$_3$Enterobactin (FeH$_3$EB) fragments based on MALDI-TOF MS spectra [1], calculated using minimum and maximum atomic weights (ma) from the IUPAC 2013 technical report [12] and monoisotopic mass Mm [16]. m_a(H)= [1.00784, 1.00811]; m_a(C)[12.0096, 12.0116], m_a(N)[14.00643, 14.00728], m_a(O)[15.99903, 15.99977], m_a(Na) [22.98977] and m_a(Fe)[55.845] were considered in the estimation of minimum and maximum molecular weights (Mw), and Mm was calculated using web tool provides by http://www.cheminfo.org. Being the average of the mass measurement error (or accuracy) of Δm:11.625 ppm (0.0011%) [16].

leave the bond C5–C4 more reactive than C4-N in H_6EB (see Figs. 2 and 3). This is reflected in the dependence of frontier orbitals (HOMO-LUMO) with the frequency distribution of catecholamide dihedral angles of H_6EB depicted in Figs. 4-8, for five H_6EB structures. Despite of this wide versatility, the catecholamide arms tend to converge in only one range of frequencies; from − 60° to 60°, granting to H_6EB a predominant reactive region governed for carbonyl groups (amide and ester). This match with the C4-N scission reveled from the MALDI-TOF MS data [1]. Fig. 8 depicts the highest occupied molecular orbital (HOMO) and lowest occupied molecular orbital (LUMO) of H_6EB structures, where the effects of the dihedral angles are evident. They show an asymmetrical distribution of the ability to donate electrons (HOMO) and accept electrons (LUMO) located in the catecholamides arms.

Based in other analyzes by Vonlanthen et al. [13] and Mishchenko et al. [14] for a study of molecular conductance in a series of organic molecules with fixed dihedral angles, it is expected that

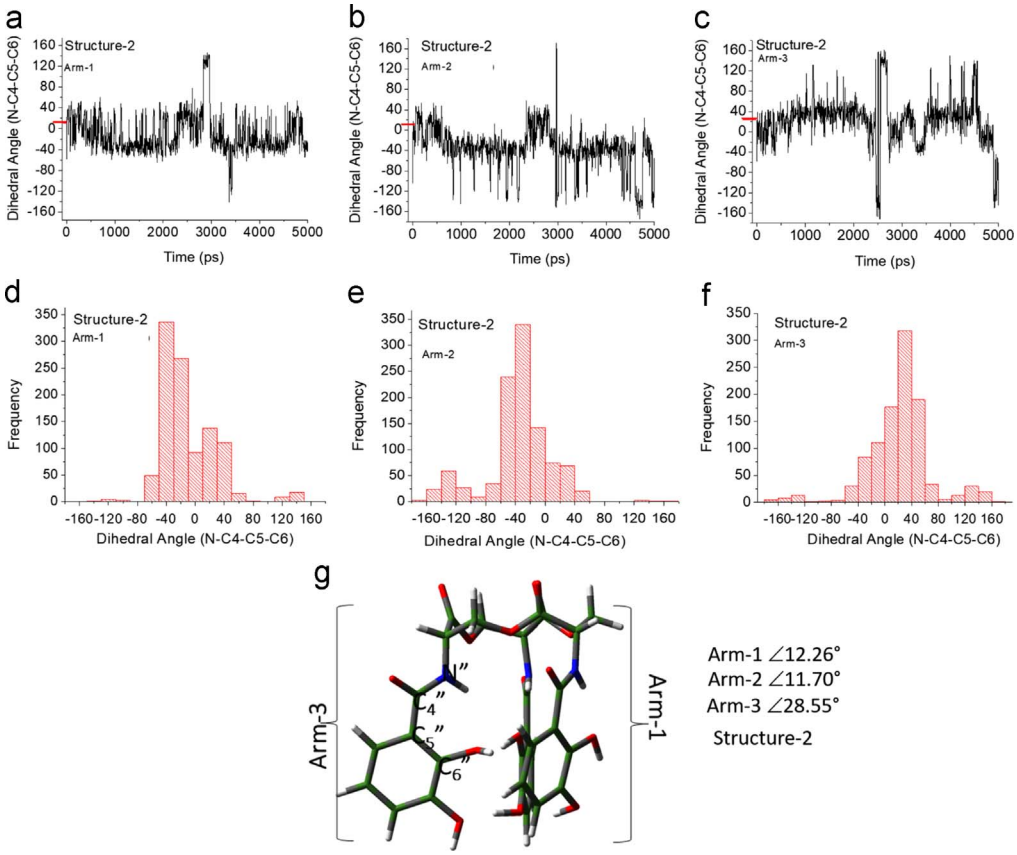

Fig. 4. Dihedral angles of structure-2 arms (g) as a function of time (a-c) and frequency distribution (d-f).

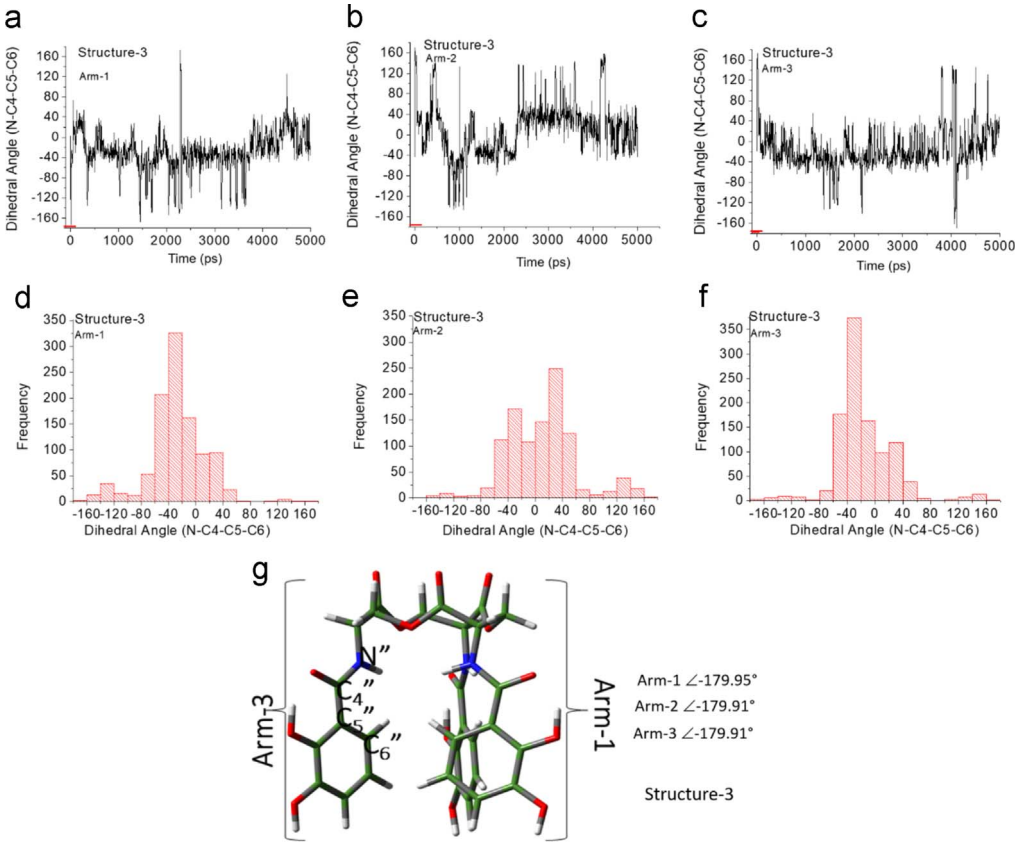

Fig. 5. Dihedral angles of structure-3 arms (g) as a function of time (a-c) and frequency distribution (d-f).

the dihedral angles influence the properties of siderophores and their analogs as reported by Raymond et al. [15].

Thus, data here allow us to infer that the IR spectra and the reactivity are strongly influenced by the presence of Fe. These, together with the steric effects between the arms of catecholamide and with the trilactone backbone, as it is showed in data here. The reactive regions in $[CatFeEB]^{3-}$ and H_6EB, where the delocalization of electrons (amide, esters, and catechol groups) is predominant, are like a protein recognition code, giving rise to cellular memory. Nevertheless, this is beyond the scope of this contribution.

2. Experimental design, materials, and methods

Experimental infrared spectra were recorded at 50000 scans recorded with $2\,cm^{-1}$ resolution. Samples, $[SalFeH_3EB]^0$ and H_6EB, were measured using KRS-5 disc. Fifty milligrams of $[SalFeH_3EB]^0$

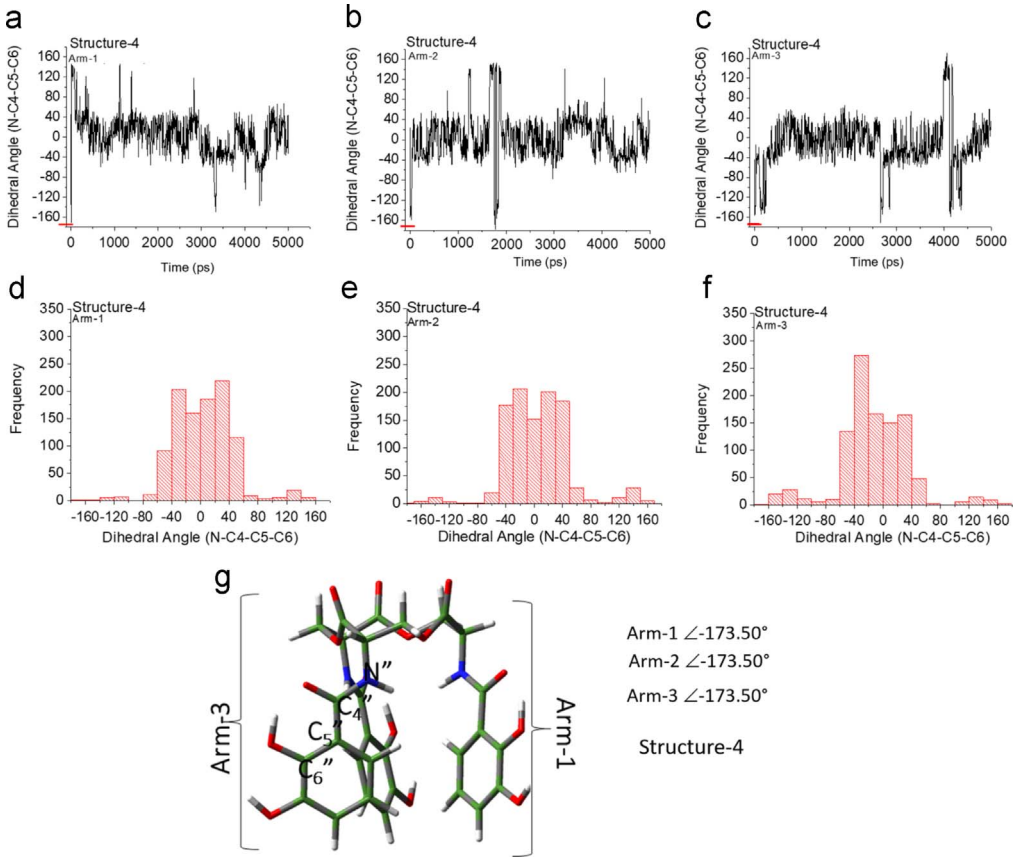

Fig. 6. Dihedral angles of structure-4 arms (g) as a function of time (a-c) and frequency distribution (d-f).

and H_6EB, separately, was dispersed in 100 μl of dichloromethane, then one drop was placed on a KRS-5 disc to dry. Solid H_6EB and $[SalFeH_3EB]^0$ were characterized. All solvents and H_6EB were of analytical purity. For the sample preparation of MALDI-TOF MS spectra, 0.5 mL of a saturated solution of a-cyano-4-hydroxycinnamic acid (HCCA) in acetone was deposited on the sample target. A 1 ml aliquot of the sample was injected into a small drop of water previously deposited on the matrix surface.

Quantum Chemical calculations were performed using Density Functional Theory (DFT) with the PBE exchange-correlation functional including long-range corrections [6] and QZVP [7,8] basis sets, with an ultrafine integral grid. Different starting catechol amide dihedral angles of H_6EB were considered for the calculations (see data in Figs. 3-6). All the results presented correspond to a local minimum for each of the calculated structures. All theoretical results were performed with the Gaussian 09 code [9] and we used Gauss-View to visualize the molecular

orbitals, electrostatic potentials, and the vibrational modes. To obtain the frequencies of different dihedral angles values (Arm1, Arm2, and Arm3) from H_6EB structures over a time lapse, molecular dynamics (MD) simulations (using the Desmond code) of the four structures of H_6EB were performed, where each structure was embedded into an explicit TIP3P [2] water box. The NPT ensemble was employed with at 300 K and 1.01 bar of pressure and the OPLS-2005 force field [3] was used. Each system was subjected to energy minimization before the MD simulations were carried out for 5 ns. We used a VMD software [5] to calculate the dihedrals angles on catecholamides from H_6EB structures during the MD trajectories. Plots were done with Origin 6.0 (OriginLab, Northampton, MA). All systems were simulated considering periodic boundary conditions (PBC).

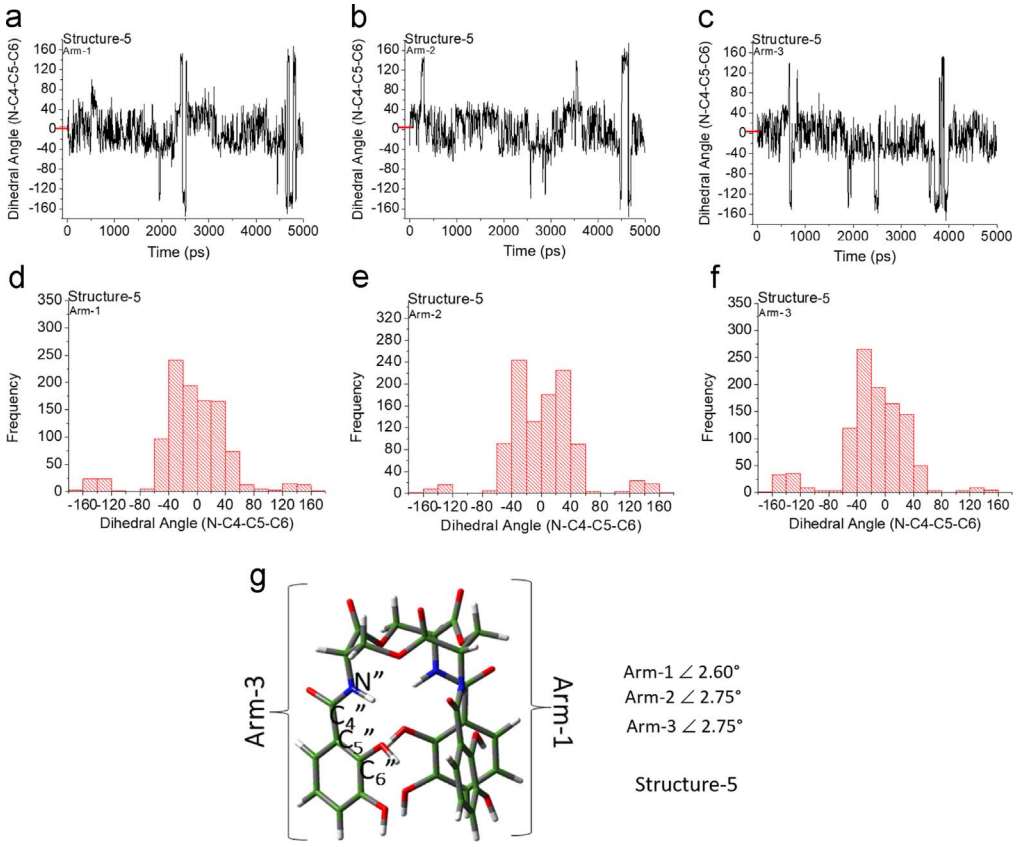

Fig. 7. Dihedral angles of structure-5 arms (g) as a function of time (a-c) and frequency distribution (d-f).

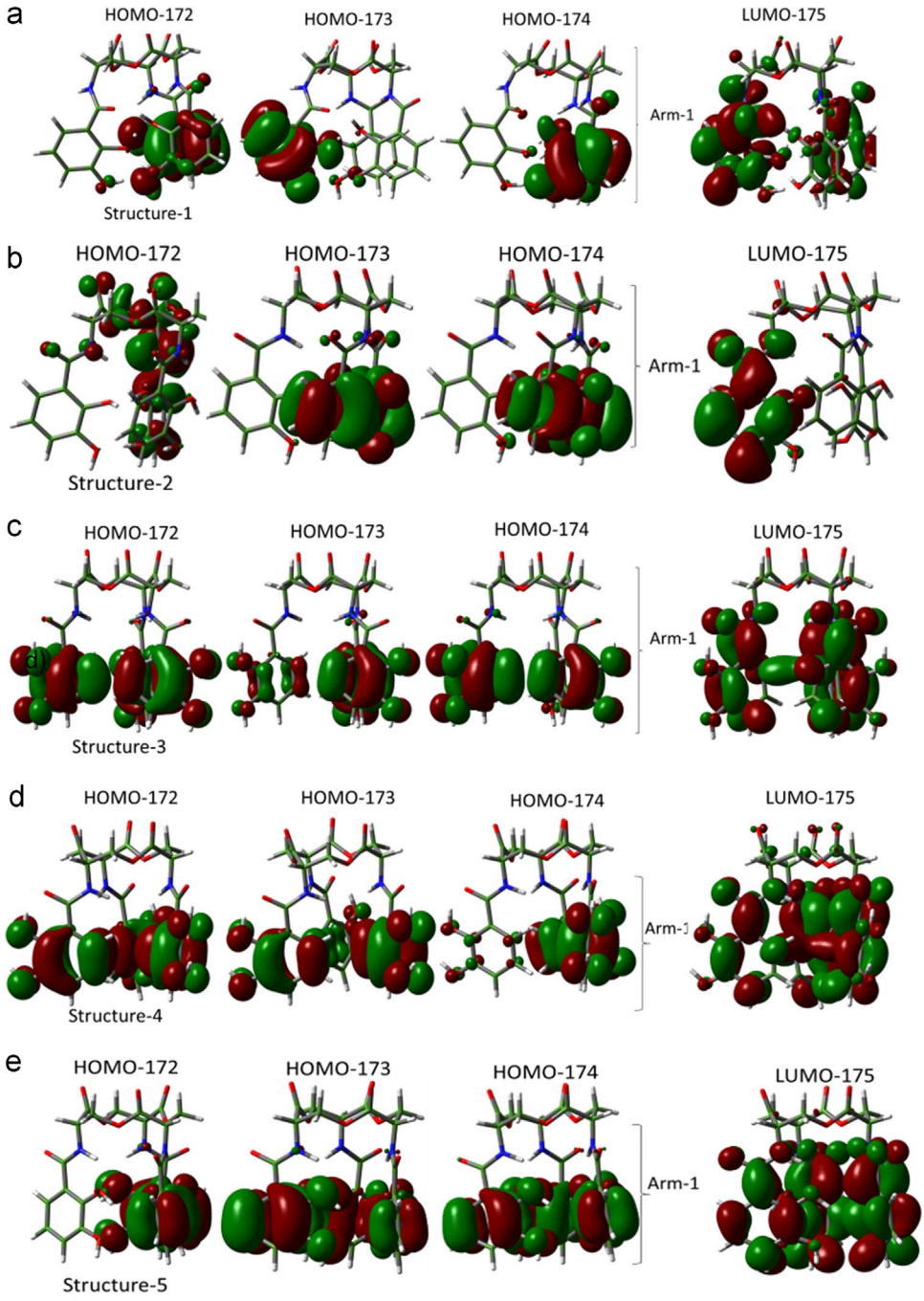

Fig. 8. Frontier Orbitals (HOMO-LUMO) of structure 1(a), structure-2(b), structure-3(c), structure-4(d) and structure-5(e).

Acknowledgments

We thank next funding sources; Lamellar Nanostructure and Bio Nanomedicine groups of the Center for the Development of Nanoscience and Nanotechnology (CEDENNA) Chile, and the Experimental II Department of the Max Planck Institute for Microstructure Physics in 2011.

ACT-1107 Project titled “Integration of Structural Biology to the development of Bionanotechnology” funded by CONICYT, Chile. FGN acknowledge the support of FONDECYT Grant 1170733 and MAA is funded by CONICYT PCHA/Doctorado Nacional 2017-21172039 fellowship. The Centro Interdisciplinario de Neurociencia de Valparaíso (CINV) is a Millennium Institute supported by the Millennium Scientific Initiative of the Ministerio de Economía, Fomento y Turismo.

We also thank the Computer facilities of the MPI Halle and the CBIB of Universidad Andres Bello, and Dr. Andrea Porzel from Leibniz Institute of Plant Biochemistry for help with MALDI-TOF MS interpretation.

Transparency document. Supporting information

Transparency data associated with this article can be found in the online version at https://doi.org/10.1016/j.dib.2018.08.114.

References

[1] M. Moreno, A. Zacarias, A. Porzel, A. Velasquez, G. Gonzalez, M. Alegría-Arcos, F. Gonzalez-Nilo, E.K.U. Gross, IR and NMR spectroscopic correlation of enterobactin by DFT, Spectrochim. Acta A 18 (2018) 264–277.
[2] W.L. Jorgensen, J. Chandrasekhar, J.D. Madura, R.W. Impey, M.L. Klein, Development of an improved four-site water model for biomolecular simulations: tip4p-ew, J. Chem. Phys. 79 (1983) 926–935.
[3] W.L. Jorgensen, D.S. Maxwell, J. Tirado-Rives, Development and testing of the OPLS all-atom force field on conformational energetics and properties of organic liquids, J. Am. Chem. Soc. 118 (1996) 11225–11236.
[4] Desmond Molecular Dynamics System, Desmond Molecular Dynamics System Version 3.6, D.E. Shaw Research, New York, NY., 2013.
[5] W. Humphrey, A. Dalke, K. Schulten, VMD: visual molecular dynamics, J. Mol. Graph. 14 (1996) 33–38.
[6] J.P. Perdew, K. Burke, M. Ernzerhof, Phys. Rev. Lett. 77 (1996) 3865–3868.
[7] F. Weigend, R. Ahlrichs, Balanced basis sets of split valence, triple zeta valence and quadruple zeta valence quality for H to Rn: design and assessment of accuracy, Phys. Chem. Chem. Phys. 18 (2005) 3297–3305.
[8] F. Weigend, F. Furche, R. Ahlrichs, Gaussian basis sets of quadruple zeta valence quality for atoms H–Kr, J. Chem. Phys. 24 (2003) 12753–12762.
[9] J. Frisch, et al., Gaussian 09, revision B.01, Gaussian Inc., Wallingford CT, 2010.
[10] V.L. Pecoraro, W.R. Harris, G.B. Wong, C.J. Carrano, K.N. Raymond, Coordination chemistry of microbial iron transport compounds. 23. Fourier transform infrared spectroscopy of ferric catechoylamide analogues of enterobactin, J. Am. Chem. Soc. 14 (1983) 4623–4633.
[11] W.R. Harris, C.J. Carrano, S.R. Cooper, S.R. Sofen, A.E. Avdeef, J.V. McArdle, K.N. Raymond, Coordination chemistry of microbial iron transport compounds. 19. Stability constants and electrochemical behavior of ferric enterobactin and model complexes, J. Am. Chem. Soc. 20 (1979) 6097–6104.
[12] M.E. Wieser, N. Holden, T.B. Coplen, J.K. Böhlke, M. Berglund, W.A. Brand, P. De Bièvre, M. Gröning, R.D. Loss, J. Meija, T. Hirata, Atomic weights of the elements 2011 (IUPAC Technical Report), Pure Appl. Chem. 5 (2013) 1047–1078.
[13] D. Vonlanthen, A. Mishchenko, M. Elbing, M. Neuburger, T. Wandlowski, M. Mayor, Chemically controlled conductivity: torsion-angle dependence in a single-molecule biphenyldithiol junction, Angew. Chem. Int. Ed. 48 (2009) 8886–8890.
[14] A. Mishchenko, L.A. Zotti, D. Vonlanthen, M. Bürkle, F. Pauly, J.C. Cuevas, M. Mayor, T. Wandlowski, Single-molecule junctions based on nitrile-terminated biphenyls: a promising new anchoring group. Single-molecule junctions based on nitrile-terminated biphenyls: a promising new anchoring group, J. Am. Chem. Soc. 133 (2010) (184-1187).
[15] T.M. Hoette, R.J. Abergel, J. Xu, R.K. Strong, K.N. Raymond, The role of electrostatics in siderophore recognition by the immunoprotein siderocalin 1, J. Am. Chem. Soc. 51 (2008) 17584–17592.
[16] L. Patiny, A. Borel, ChemCalc: a building block for tomorrow’s chemical infrastructure, J. Chem. Inf. Model. 53 (2013) 1223–1228.